LAWRENCE
LIVERMORE
NATIONAL
LABORATORY

LLNL-TR-739186

DOE FES FY2017 Joint Research Target Fourth Quarter Milestone Report for theNational Spherical Torus Experiment Upgrade.

V. A. Soukhanovskii

September 29, 2017

Disclaimer

This work performed under the auspices of the U.S. Department of Energy by Lawrence Livermore National Laboratory under Contract DE-AC52-07NA27344.

Fusion Energy Sciences
FY 2017 Joint Research Target (JRT)
Fourth Quarter Milestone Report
National Spherical Torus Experiment Upgrade

Executive summary

A successful high-performance plasma operation with a radiative divertor has been demonstrated on many tokamak devices, however, significant uncertainty remains in accurately modeling detachment thresholds, and in how detachment depends on divertor geometry. Whereas it was originally planned to perform dedicated divertor experiments on the National Spherical Tokamak Upgrade to address critical detachment and divertor geometry questions for this milestone, the experiments were deferred due to technical difficulties. Instead, existing NSTX divertor data was summarized and re-analyzed where applicable, and additional simulations were performed.

Divertor studies in the *geometrically open* standard divertor configuration in NSTX can be summarized as follows:

- Core density ramps up to the Greenwald density did not produce outer strike point detachment;
- Stable outer strike point partial detachment was obtained only with additional divertor gas injection;
- Midplane gas injection at the same rate (cf. divertor gas injection) resulted in transient partial detachment during the gas flow, and re-attachment without the gas flow;
- Access to stable partial outer strike point detachment was facilitated in the strongly shaped plasmas.

These finding suggest a way to optimize the open divertor for partial outer strike point detachment, by placing the neutral gas source in the vicinity of the strike point, directing the recycling neutrals toward the separatrix (by adjusting the poloidal separatrix angle), and entrapping the neutrals in the high poloidal flux expansion configuration (via plasma plugging).

Significant attention has been given to trying to understand the power scrape-off layer (SOL) width, λ_q, and how it scales to larger more powerful tokamaks. Due to their compact nature, spherical tokamaks (STs) may need to operate in a double-null (DN) configuration to

reduce heat fluxes on plasma facing components (PFCs). However, tokamaks with a larger aspect ratio have been primarily focused on lower single null (LSN) discharges which is the baseline operating scenario for ITER. Consequently, few experiments have focused on λ_q behavior in DN scenarios. Results presented here show distinct differences between LSN and DN plasmas. The S parameter, which describes how much incident heat flux diffuses into the private flux region, is found to be systemically higher in LSN than in DN NSTX plasmas. While λ_q itself remains unchanged between LSN and DN plasmas. A minimum in power deposited onto the lower, outer strike point of 10 – 25% P_{SOL} is found when $-2 \leq \delta_r^{sep}/\lambda_{q||,\,OMP} \leq 2$, i.e. very near DN. Full power accounting in NSTX-U is planned for increased IR coverage of all divertor strike points.

Introduction

Based on nearly five decades of magnetically confined nuclear fusion plasma physics research, an axisymmetric poloidal magnetic X-point divertor has emerged as the most promising vision for a tokamak plasma-material interface (PMI). The poloidal divertor enables energy and particles lost from the confined core plasma due to radial transport and magnetohydrodynamic (MHD) instabilities (e.g., edge localized modes (ELMs)) to flow to the divertor chamber, which acts as a separate plasma-material interface. Cross-field transport in the edge and scrape-off layer (SOL) is generally anomalous (higher than collisional (Bohm) transport enhanced by neoclassical effects). Recent work highlights the intermittent nature of SOL transport: filamentary structures carry particles at high rates in the SOL. The divertor SOL parallel heat transport is dominated by electron conduction and convection and strongly depends on plasma collisionality. At higher plasma collisionality, a low-temperature highly radiative divertor plasma regime sets in: the plasma flowing to divertor plates loses energy through radiation and dissipative processes, and momentum through charge exchange, inelastic collisions and recombination. This leads to significant plasma neutralization before contacting the divertor plate surface (i.e., detachment), and, as a result, significantly reduced heat load and material erosion. This radiative regime is commonly called radiative plasma detachment, or divertor detachment. It is characterized by a parallel SOL electron (plasma) pressure drop, high neutral divertor pressure (density), low plasma electron temperature ($T_e \leq$ 1-2 eV) and high electron density at the plate, leading to high impurity radiation. Divertor detachment is viewed as the primary potential solution to tokamak power and particle exhaust given our present understanding of the operating limits of plasma-facing component cooling technology and target materials. The proposed ITER divertor is based on standard X-point divertor geometry designs tested in large tokamak experiments: vertical targets with partial radiative detachment of the strike points are envisioned.

The NSTX Upgrade restarted plasma operations in FY2016. In preparations for the FES Joint Research Target 2017, several experiments had been proposed at the Research Forum that took place in February 2015. However, because of technical difficulties encountered with plasma operations in FY2016, the divertor experiments were not executed. The main contribution from the NSTX Team toward the FES Joint Research Target was therefore based on analysis of NSTX

divertor experiments as well as modeling of the NSTX results.

In addition to the NSTX divertor analysis, an experiment was executed on DIII-D by NSTX-U staff within the NSTX-U experimental campaign in June 2017. The experiment "Divertor detachment studies in highly-shaped NSTX/NSTX-U-like plasmas" was aimed at comparison of divertor detachment onset and characteristics between NSTX and DIII-D. Results from this experiment are also included in the report.

NSTX lower single null divertor data analysis

Experiments were executed in NSTX in 2004-2010 to apply the radiative divertor technique to the spherical torus for the first time, and study radiative detachment operating space and its characteristics. NSTX had an open divertor geometry with a horizontal and slightly tilted (15 degrees to horizontal) outer target with graphite PFCs. Divertor experiments in NSTX spanned a range of plasma shaping parameters which can be grouped into weakly-shaped and highly-shaped plasmas. The weakly-shaped plasmas were generally more prone to MHD instabilities and were characteristic of earlier years of NSTX operations. The highly-shaped H-mode plasma scenarios were developed in later years and became a basis for high-performance long pulse H-mode. The relevant experiments are summarized below:

- XP 605, Divertor heat flux reduction and detachment in NBI-heated plasmas
    - Low triangularity $\delta \leq 0.40$ H-mode plasmas with higher strike point major radius $R_{OSP} \sim 0.75$-0.8 m, low outer strike point flux expansion
- XP 708, Divertor heat flux reduction and detachment in highly shaped plasmas
    - High triangularity $\delta \leq 0.72$ H-mode plasmas with lower strike point major radius $R_{OSP} \sim 0.4$-0.5 m, high outer strike point flux expansion
- XP 814, Divertor heat flux reduction and detachment in highly-shaped high-performance plasmas
    - Extending studies from XP 708 to high-performance plasmas with plasma currents 1.0 - 1.2 MA and NBI input power $P_{NBI} \leq 6$ MW.
- XP 816, Edge characterization in highly shaped plasmas
    - Studies of divertor conditions as a function of X-point height in 4 MW NBI-heated H-mode plasmas

- XP 826, X-point limiter
    - Studies of divertor conditions in a standard divertor configuration with marginal X-point height, nearly limited by the lower X-point
- XP 1045, "Snowflake" divertor configuration in NSTX
    - Studies of a very high flux expansion snowflake-minus divertor configuration
- XP 1050, Radiative divertor with impurity seeding and lithium coatings in NSTX
    - Studies of divertor detachment in a high flux expansion standard and snowflake-minus configurations with lithium coatings and additional deuterated methane CD_4 seeding

Data from the above experiments have been analyzed and presented in conferences and peer-review publications. In this report, we summarize several points from NSTX divertor studies to address the Joint Research Target 2017 goals:

- The operating space and characteristics of a partially detached divertor in NSTX
- Dependence of partial detachment characteristics in NSTX on the divertor configuration from experiments and modeling
- Dependence of the radial extent of the partially detached region on divertor SOL width and gas seeding

Detachment operating space

Divertor heat flux reduction and detachment in NSTX were studied in the lower single null (LSN) H-mode plasma configurations with weaker shaping (elongation κ=1.8–2.0 and triangularity δ=0.4–0.5), and with stronger shaping (elongation $\kappa \leq 2.3$ and triangularity $\delta \leq 0.7$), as shown in Fig. 1 [1-3].

Additional quantities of room-temperature deuterium (D_2) were injected using gas injectors situated at various poloidal locations: at the outboard midplane, inner divertor (ID), and private flux region (PFR) locations for the low-triangularity configurations, and PFR and outer strike point region (outer SOL) for the high-triangularity configurations, as shown in Fig. 1. Both the PFR and the ID injectors were operated at steady-state rates $\sim 10^{22}$ s^{-1}. Using a different gas delivery hardware setup, the ID injector was also operated in a pulsed mode injecting deuterium from four small plenums through four toroidally symmetric ports in the divertor floor.

Each pulse duration was 15-20 ms at an average rate of (0.85 - 3.0) x 10^{22} s^{-1}. For comparison, a typical reference plasma particle inventory was in the range (7-10) x 10^{20}.

In dedicated experiments, D_2 was injected to investigate the effectiveness of the radiative and dissipative techniques for divertor heat load reduction, and the impact of additional gas puffing on confinement and plasma performance. A general result of adding deuterium injection was a reduction of the peak outer strike point heat flux by 30-80 %. As the deuterium puffing rate was increased, the outer SOL thermal electron collisionality increased from ν^*_e ~ 5-20, estimated from the Thomson scattering data at the separatrix in reference plasmas, to ν^*_e ~ 30-80. The radiative and dissipative divertor losses increased, and the outer SOL transitioned from a radiative high-recycling divertor regime to a partially detached divertor regime. An operational path to these conditions was different with each gas injector, highlighting the challenge of divertor heat flux reduction in a spherical tokamak open divertor geometry without active pumping. In the configurations with weak shaping, puffing deuterium at the midplane in 3 - 4 MW NBI heated plasmas was the least successful as an H-L back transition and large MHD modes occurred within one τ_E, with simultaneous confinement degradation to 0.6-1.0 of the ITER89P scaling, as shown in Fig. 2. However, the radiative and detached divertor operating modes, obtained with the *divertor* gas puffing at moderate and high rates produced good results, i.e. divertor heat flux mitigation with insignificant, if any, confinement degradation. In the configurations with strong shaping, similar results were obtained: the best MHD-stable H-mode discharges with a partially detached strike point were obtained only with divertor gas puffing.

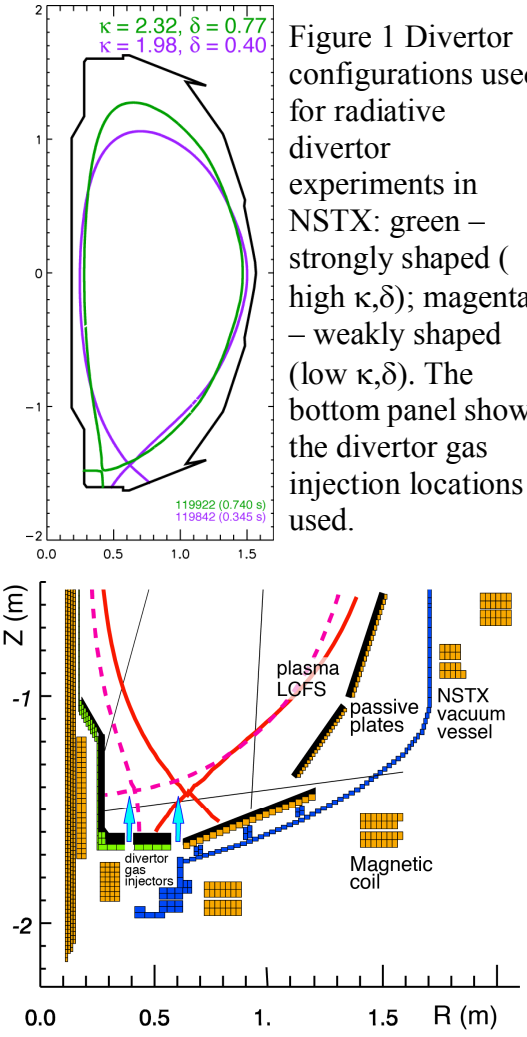

Figure 1 Divertor configurations used for radiative divertor experiments in NSTX: green – strongly shaped (high κ,δ); magenta – weakly shaped (low κ,δ). The bottom panel shows the divertor gas injection locations used.

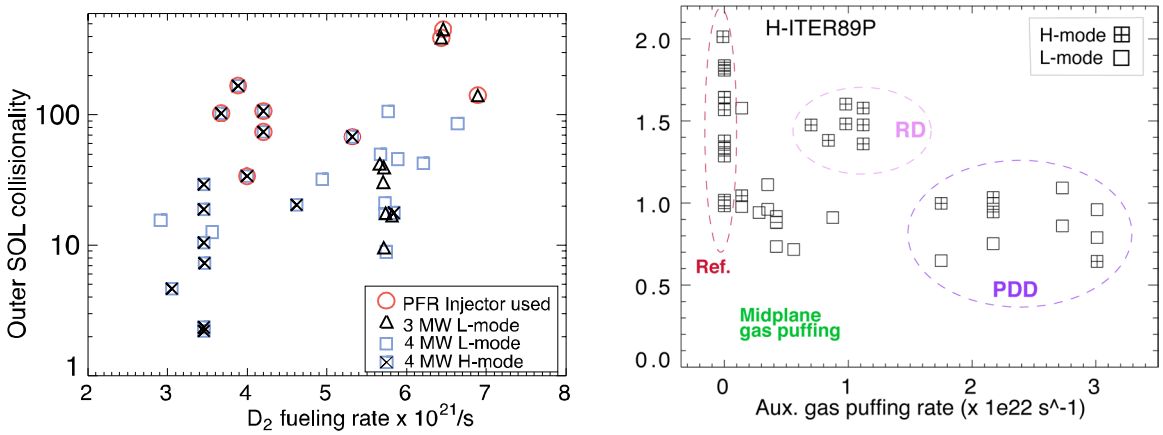

Figure 2 Normalized outer SOL collisionality (left) and the confinement H-ITER89P factor as a function of additional gas puffing in L- and H-mode plasmas in radiative divertor experiments on NSTX.

In the discharges with weak shaping, the inner divertor leg detachment occurred naturally at n_e = 2–3 x 10^{19} m^{-3} and input power $0.8 \le P_{NBI} \le 6$ MW. The inner divertor leg region remained in a detached state with $q_{in} \le 1$ MW/m^2 and T_e~1-2 eV, n_e=(0.7–4) x 10^{20} m^{-3} throughout the operating space (similar to conventional tokamaks). Inner strike point detachment was attributed to a combination of factors: the proximity of the vertical inner wall acting as a source of deuterium neutrals and carbon, a broad heat flux profile with reduced $q_{||}$, and a long connection length [4,5].

The density threshold for the outer strike point partial detachment was found to be high, as the detachment was not observed even at the plasma densities approaching the Greenwald density n_G. In NBI-heated H-mode plasmas the outer strike point peak heat flux q_{pk} demonstrated a linear scaling with the SOL power, being in the 2–12 MW/m^2 range for 1–6 MW NBI power, and

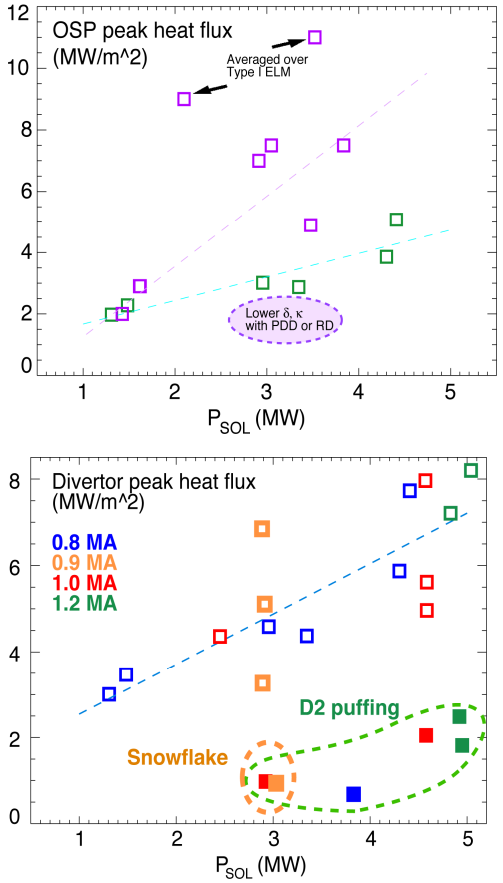

Figure 3. Peak heat flux in NSTX outer strike point as a function of scrape-off layer power for the strongly shaped and weakly shaped configurations (top), and for divertor detachment experiments (bottom)

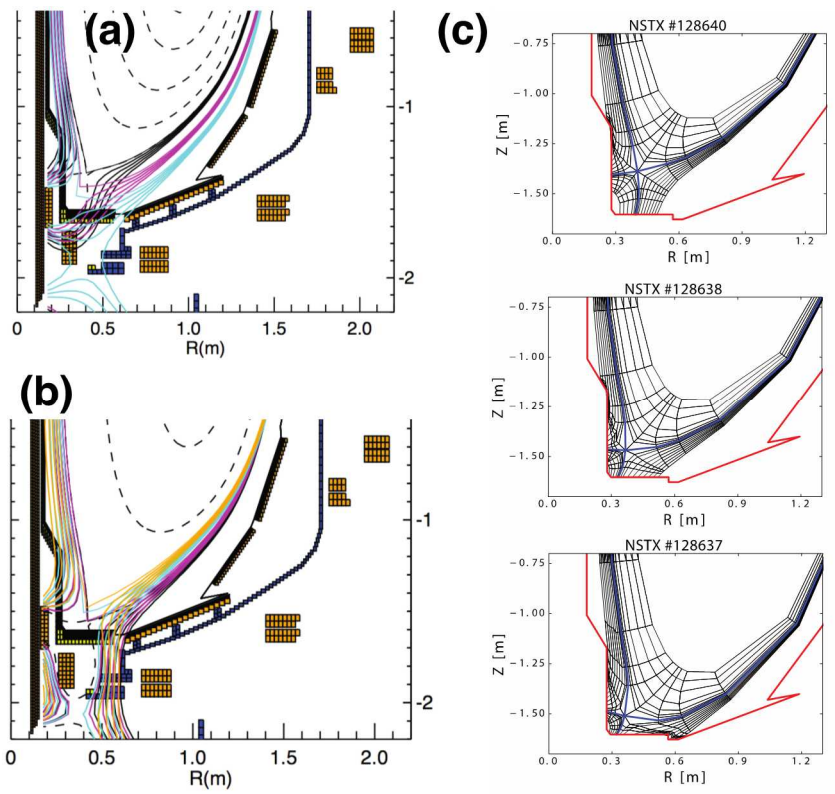

Figure 4. X-point scan experimental equilibria used to study impact of flux expansion and poloidal angle on detachment onset (a) with the same strike point radius (b) with variable strike point radius. In (c), UEDGE grids for modeling experimental results of (a) are shown (top – high X-point, medium – medium X-point height, bottom – low X-point height.

monotonically increasing with the plasma current I_p commensurate with the change in q_{95} (connection length) and SOL power width λ_q [6, 7].

Radiative divertor experiments were conducted in 4-6 MW NBI-heated H-mode discharges using D_2 injection at rates 5−29 x 10^{21} s^{-1}. In a weakly shaped configuration, a partially detached divertor regime was obtained only at high gas seeding rates 15−29 x 10^{21} s^{-1} that led to an X-point MARFE formation and confinement degradation. The limited access to detachment was found to be qualitatively consistent with predictions of zero-dimensional two point models and two-dimensional multi-fluid modeling using the UEDGE code: sufficiently high steady-state volumetric power and momentum losses required for detachment at high parallel heat flux q≤30–50 MW/m^2 in the open NSTX geometry carbon divertor with a short parallel length and poor gas entrapment was difficult to obtain. In contrast, experiments conducted in 0.8-1.2 MA, 4-6 MW NBI-heated H-mode discharges in a highly-shaped LSN configuration demonstrated reliable access to the partially detached divertor regime. The peak heat flux at the outer strike point (SP) was successfully reduced from 4-10 MW/m^2 to 0.5-2 MW/m^2 using divertor deuterium injection with minimal confinement deterioration, as summarized in Figure 3 [1-3].

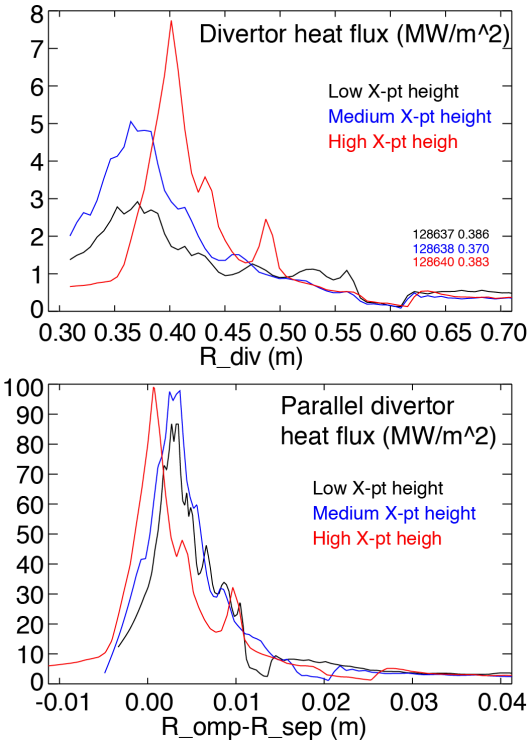

Figure 5. Divertor deposited (top) and parallel (bottom) heat fluxes in the three X-point hieigh highly shaped configurations.

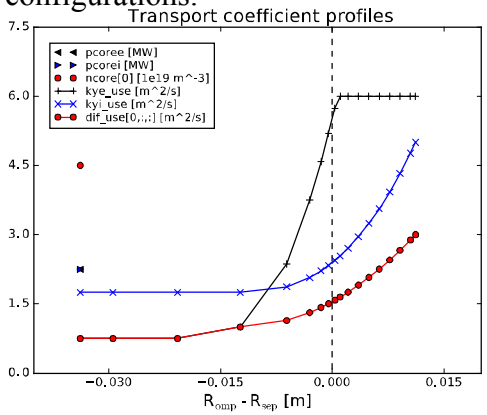

Figure 6. Radial transport coefficient profiles used in the UEDGE model. The boundary conditions for the core-boundary interface are shown: power (pcoree – for electrons, pcorei – for ions) and density (ncore). The transport coefficients are: kye – electron conductivity, kyi – ion conductivity, dif_use – effective particle diffusion.

Role of divertor geometry in detachment onset

Motivated by the above observations, the role of high flux expansion in detachment threshold was investigated in more detail. A hypothesis was put forward that a higher isothermal divertor volume and higher plasma "plugging efficiency" in the high flux expansion divertor can potentially lead to higher power P_{rad} and momentum p_m losses, thereby facilitating detachment onset. Tokamak studies conducted in open geometry unpumped graphite-tiled divertors most relevant for comparison with NSTX also support these notions. Re-ionization of recycling neutrals in the divertor chamber termed "flux amplification" is an essential feature of the high-recycling divertor regime. As the recycling is increased, the divertor density increases, the divertor temperature further decreases, leading to an increase in the P_{rad} and p_m loss factors, loss of parallel pressure balance, and a transition to detachment. The plasma "plugging efficiency" is defined as a fraction of recycling neutrals re-ionized in the divertor region. In the high flux expansion divertor it is higher because of a larger divertor plasma size in physical space with respect to ionization, charge exchange and elastic collision mean free path lengths, and higher low-temperature plasma volume. Also in this configuration, another critical factor may be the poloidal angle at which magnetic field lines hit the divertor plate. If the angle is less than 90 degrees, recycling neutrals are directed toward the separatrix, and may lead to enhanced recycling and eventually to enhanced volumetric losses

("the vertical target plate" effect). If the angle is greater than 90 degrees, the neutrals are recycled toward the outer SOL and may contribute less to ionization within the divertor. An experiment was carried out on NSTX whereby the divertor magnetic configuration geometry was systematically changed by either (i) changing the distance between the lower divertor X-point and the divertor plate (X-point height), or by (ii) keeping the X-point height constant and increasing the outer SP radius. Shown in Fig. 4 are the experimental equilibria and numerical grids used for modeling divertor transport and radiation in these configurations. The experiment was carried out in a LSN configuration, in 1 MA, 6 MW NBI-heated H-mode plasma discharges, fueled by deuterium from a high field side gas injector. For the divertor plasma analysis, infrared thermography, spectrally filtered cameras, divertor bolometers, a multi-channel UV-visible spectrometer, and Penning and micro-ion neutral pressure gauges were used. Experimental

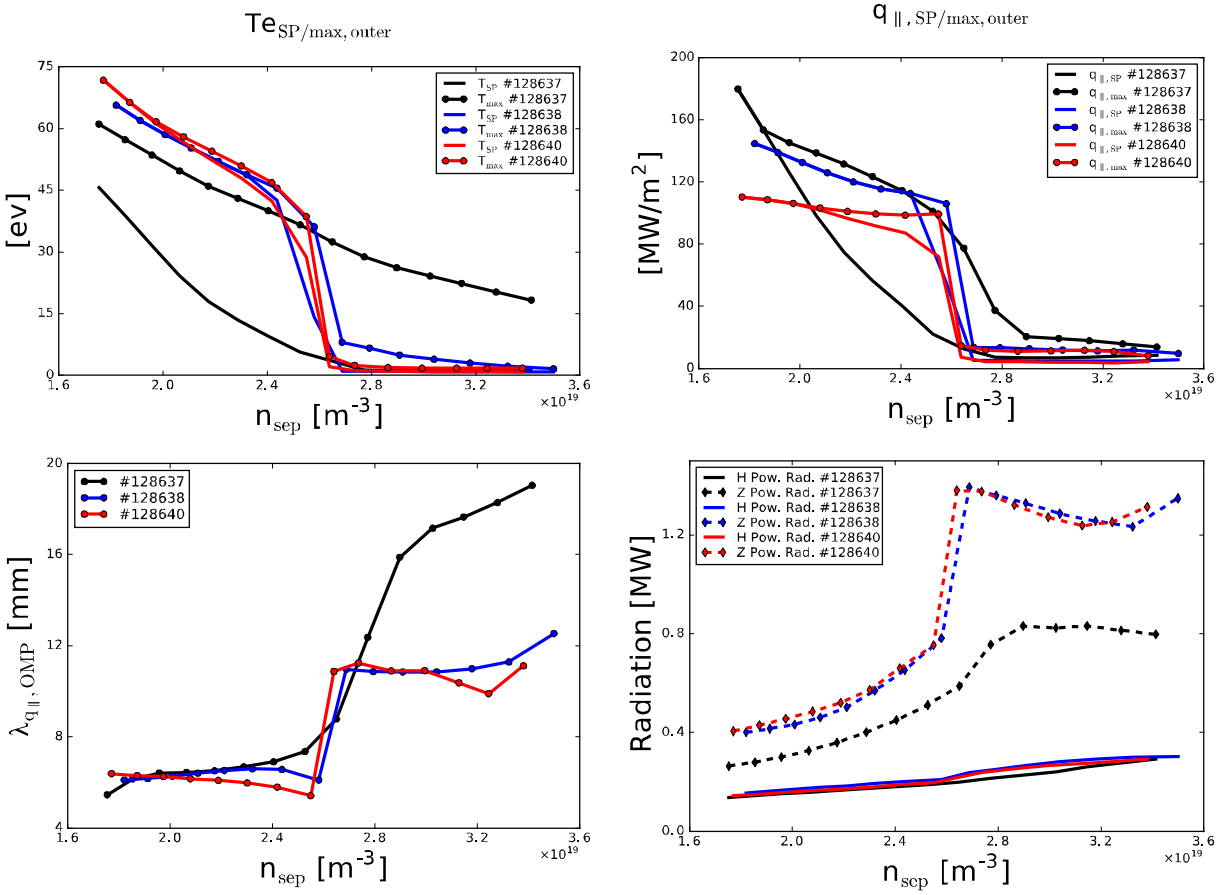

Figure 7. Density scans of divertor T_e, divertor parallel heat flux, divertor power width, and divertor radiation as functions of n_{sep} in UEDGE models.

divertor data analysis was previously presented [8] and is summarized below. Additional analysis included modeling of divertor transport and radiation with the multi-fluid code UEDGE and is also summarized below.

Divertor heat flux profiles measured in the three X-point height configurations are shown in Fig. 5. The parallel divertor heat flux was slightly lower in the highest flux expansion configuration. While the divertor poloidal magnetic flux expansion factor appeared to play the dominant role in peak divertor heat flux reduction from 7-8 MW/m^2 to 1-2 MW/m^2, the higher flux expansion configurations also showed higher impurity emission and a higher deuterium high-*n* line emissions indicative of higher recombination rates [8]. These experimental observations suggested that the lower X-point height configuration facilitated detachment of the outer strike point region.

In order to understand the experimental results, UEDGE code modeling of each configuration was performed. The goal of the simulations was to evaluate how each configuration approaches detachment with increasing upstream density. The model included the core-boundary power of 4.6 MW equally divided between electrons and ions. It was assumed that radial heat and particle transport (including impurities) was not modified by the divertor configurations: the same radially varying transport coefficients were used for all three configurations. The radial transport coefficient profiles are shown in Fig. 6. The divertor plate recycling was 0.999, the wall recycling coefficient was 0.90, both the physical and chemical sputtering was used on all boundary surfaces. The carbon impurity (Z=6) was included, with cross-field particle diffusivity for all charge states set at 0.5 m^2/s. First, the medium X-point height configuration (128638) was simulated in order to find the boundary conditions and radial transport coefficients that would produce a model with upstream and divertor conditions similar to the experimental ones. These conditions included upstream radial n_e, T_e and T_i profiles, outer midplane separatrix n_e, T_e values, divertor heat flux profiles $q_{perp}(R)$, parallel divertor heat flux profiles remapped to the outer midplane, and the SOL power width. The transport and boundary model was then applied with minimal modifications to the other two divertor geometry configurations.

The modeling results can be summarized as follows (Fig. 7): using an upstream density scan that started at a low density n_{sep}=1.7 x 10^{19} m^{-3} and ended at a high density n_{sep}=3.5 x 10^{19} m^{-3}, it was demonstrated that all three configurations transition from the sheath-limited high

divertor temperature regime to the high-recycling regime and then to the partial outer strike point detachment. However, the dynamics of the approach to detachment was different. In the medium and the high X-point height configurations as the upstream density increased, divertor temperature and heat flux decreased and radiated power slowly increased. At some threshold n_{sep} value a transition to an outer strike point detachment occurred: divertor plasma parameters changed abruptly and significantly (this colloquially referred to as a "cliff"-like behavior). The low X-point height configuration, on the contrary, demonstrated a slow approach to the low divertor T_e, q_{perp} values. This is quite consistent with the experiment where this configuration showed lower parallel heat flux and increased impurity and Balmer emissions.

The SOL power width and the radial extent of the partially detached (dissipative) region.

As demonstrated by the DOE Joint Research Target 2010 activities and related experiments and modeling, the SOL power width in NSTX and other tokamaks inversely scales with plasma current (or more specifically, the outer midplane poloidal field). On-going experiments, modeling and theory attempt to connect this scaling to (neo)classical drifts, turbulent transport, or edge MHD activity. In NSTX, divertor detachment experiments were conducted in 0.8-1.2 MA discharges in the same high flux expansion divertor configuration in 4-6 MW H-mode discharges with varying divertor gas puffing. Our recent analysis attempted to connect divertor detachment characteristics to the SOL width and transport using the NSTX experimental database with I_p=0.8,

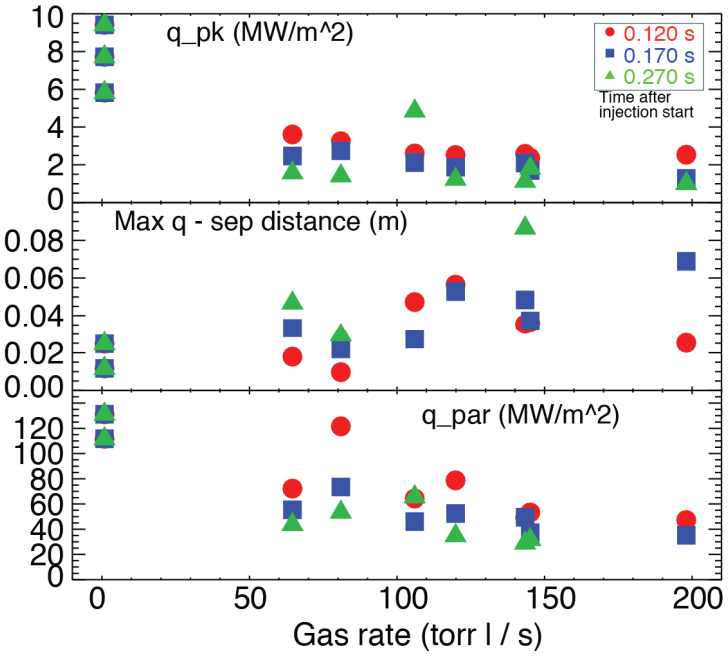

Figure 8. Divertor peak heat flux, distance between separatrix and peak heat flux (approximating the radial extent of dissipative losses), and parallel peak heat flux, as a function of deuterium injection rate for a 1.0 MA H-mode NSTX discharge

0.9, 1.0, and 1.2 MA.

A partial detachment of the outer trike point has been obtained at several deuterium injection rates for 0.8, 1.0 and 1.2 MA H-mode discharges. The divertor deuterium injector was used. An example of data analysis for 1.0 MA discharges is shown in Fig. 8: peak divertor heat fluxes, distance of peak divertor heat flux from separatrix, and peak parallel heat fluxes as functions of gas injection rate are shown for three times since the start of the gas injection. General trends can be seen with increasing gas injection: with higher rates, both parallel and deposited peak heat fluxes are reduced, and the partial detachment (dissipative loss) radial extent (approximated by the distance between the divertor heat flux peak and the separatrix) increased. The same trend is generally observed for each gas injection rate with continuing injection, as shown by three time points of different color, as the injected gas remained in the divertor due to the lack of cryo-pumping. Some discharges were disrupted by continuing gas injection which explains some missing points (e.g., the green points corresponding to later times). A similar trend is observed for 0.8, 1.0, and 1.2 MA, for which SOL power widths vary in the range λ_q= 4-8 mm [6,7]. With 6 MW NBI heating, 4-5 MW of power flows into the SOL. The λ_q scales inversely with plasma current: $\lambda_q = 0.91\ I_p^{-1.6}$ [7] and the parallel length is proportional to I_p. The relevant NSTX data is summarized in Table 1. The hypothesis was that the radial extent of the partially detached (or dissipative loss) region can be connected to the SOL power width λ_q using the characteristic dissipative connection length predicted by a one-dimensional radiative detachment model [3]. However, the scatter in the NSTX database precluded any clear trends in the data. A dedicated experiment with well-controlled divertor configuration parameters, such as steady-state strike and X-point positions, must be carried out in NSTX-U to test the hypothesis.

I_p (MA)	λ_q (mm)	$L_{\parallel}$ (m)	q_{peak} (MW/m^2)	$q_{\parallel}$ (MW/m^2)	Δ_{diss} (mm)
0.8	13	4.0	4-6	100	20-80
1.0	9	4.0-4.5	5-7	100-150	20-80
1.2	7	2.3-4.0	7-10	100-200	20-80

Table 1 Summary of NSTX LSN high-triangularity divertor parameters.

Results from the DIII-D experiment MP2017-08-02 "Divertor detachment studies in highly-shaped NSTX/NSTX-U-like plasmas"

To compare divertor detachment operating space in NSTX and DIII-D, a dedicated experiment was developed and run at DIII-D in June 2017. An NSTX-like high-triangularity double null shape with strong bias toward the lower divertor (and ion grad B drift toward the lower divertor), and with high divertor poloidal flux expansion, was developed as shown in Fig. 9. An H-mode 1 MA plasma scenario with 5 MW NBI was used to study how divertor detachment characteristics depend on the poloidal gas injection location. Three gas injectors were used, as shown in the Figure 9: one midplane injector, one far-SOL injector, and one divertor injector in the visinity of the outer strike point.

Denisty control in the discharges with gas puffing proved to be difficult as the lower cryo-pump was not used in this experiment. The experiment aimed at using the H-mode with basic lower density and additional gas injection rate ramps from 0 to 150 Tor l/s. It was

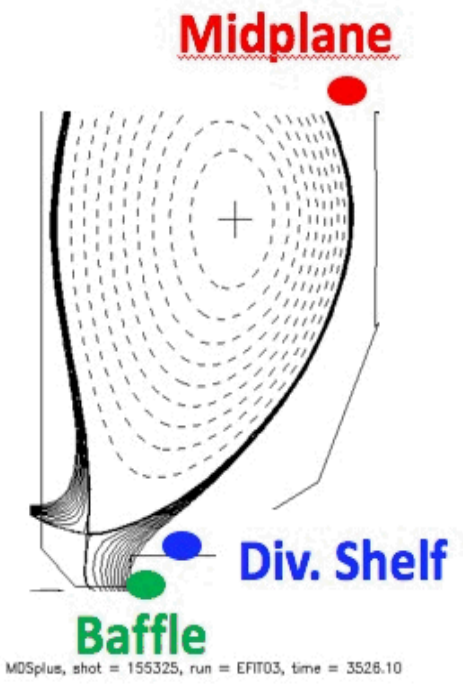

Figure 9. A schematic of the NSTX-like shape and gas injector locations that were used to study detachment similarities.

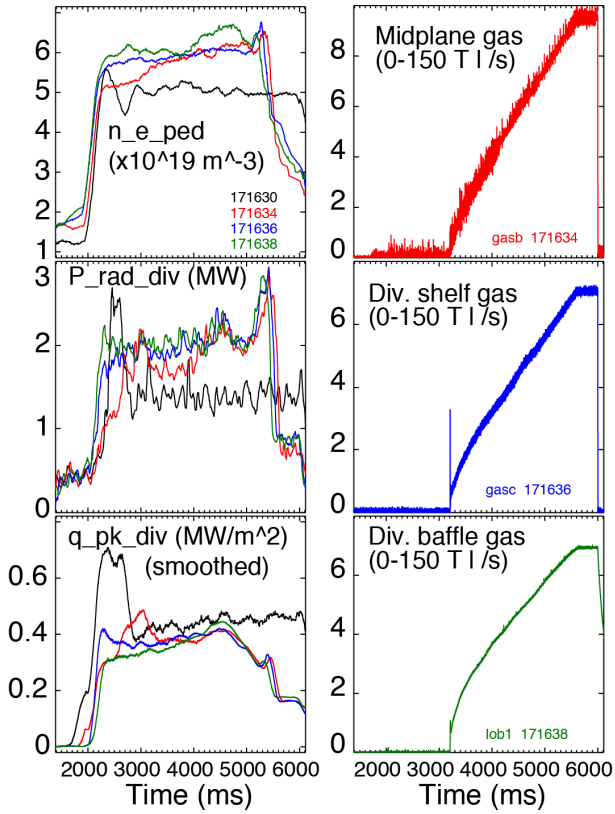

Figure 10. Time traces of pedestal density, lower divertor radiated power, divertor peak heat flux, and the three gas valves used.

expected that at some point in the ramp, the increasing density would reach the detachment onset threshold. The results showed that, generally, access to the lower outer strike point detachment had little dependence on the poloidal gas seeding location. This is summarized in Fig. 10, where time traces of four discharges are compared: one reference lower density H-mode without additional gas puffing, and three H-modes with gas puffing rate ramps from different locations. There are slightly different sensitivities of pedestal densities with additional gas puffing, however, generally, the outer strike point detachment onset occurs at about the same time (4500 ms). The heat flux profiles from IRTV, divertor Balmer emission, divertor C III and D_α profiles and Langmuir probes inicated that a partial detachment was induced with each of the three injectors at about the same time. These results suggest that access to partial detachment at DIII-D is qualitatively closer to the two-point divertor model description than in NSTX: gas injection at any location increses the SOL density and which leads to a faster divertor density rise and a transition to the detachment. In NSTX, H-mode plasmas are much more sensitive to the gas puffing location, and there is a weaker dependence of n_{sep} on the core/pedestal density and gas puffing.

NSTX Double-null divertor analysis

NSTX-U is expected to produce significant unmitigated divertor heat fluxes with a narrow SOL power width, λ_q at its designed operating parameters [11] of I_p = 2 MA and P_{NBI} = 10 MW with discharges lasting up to 5 seconds. Because of this, double-null discharge scenarios in combination with other heat flux mitigation techniques (X-Divertor, Snowflake Divertor and divertor impurity injection) will be needed to maintain divertor heat fluxes below the thermal and mechanical design limits of the plasma facing components (PFCs).

Many studies of double-null discharges were carried out on NSTX. In one such study [12] it was found that the ELM regime of the discharge changed with δ_r^{sep}, which is defined as the distance at the outer midplane between the separatrix flux surfaces passing through the upper and lower X-points, with the convention that a negative δ_r^{sep} favors the lower divertor. Because of the changing ELM regimes, measurements of the divertor heat flux must be > 1 kHz to differentiate the inter-ELM from the ELM heat fluxes. The work presented in this report is

focused on a set of discharges obtained during the 2010 run campaign of NSTX with the use of a fast [13], dual-band [14] infrared camera to be able to resolve the ELM and inter-ELM divertor heat fluxes, while δ_r^{sep} was systematically varied.

The discharges had I_p = 0.9 MA, δ_{bot} ~ 0.8 with P_{NBI} = 4 MW and utilized ~ 100 mg of lithium evaporation prior to each discharge. However, close to double-null, there was significant variation in both of δ_r^{sep} and δ_{bot}. Figure 11a shows the peak heat flux on the lower divertor at the outer strike point measured using the dual-band IR camera system to account for emissivity changes due to the use of evaporative lithium coatings. The power passing through the last closed flux surface into the SOL, P_{SOL} which is defined as $P_{SOL} = P_{NBI} + P_{oh} - \frac{dW}{dt} - P_{rad}^{core}$ is shown in Fig. 11b. P_{NBI} is the injected neutral beam power. P_{oh} is the ohmic power. dW/dt is the time rate of change of the plasma energy and P_{rad}^{core} is the power radiated from the core plasma. Figure 11c and 11d show the value of δ_r^{sep} derived from an EFIT02 magnetic

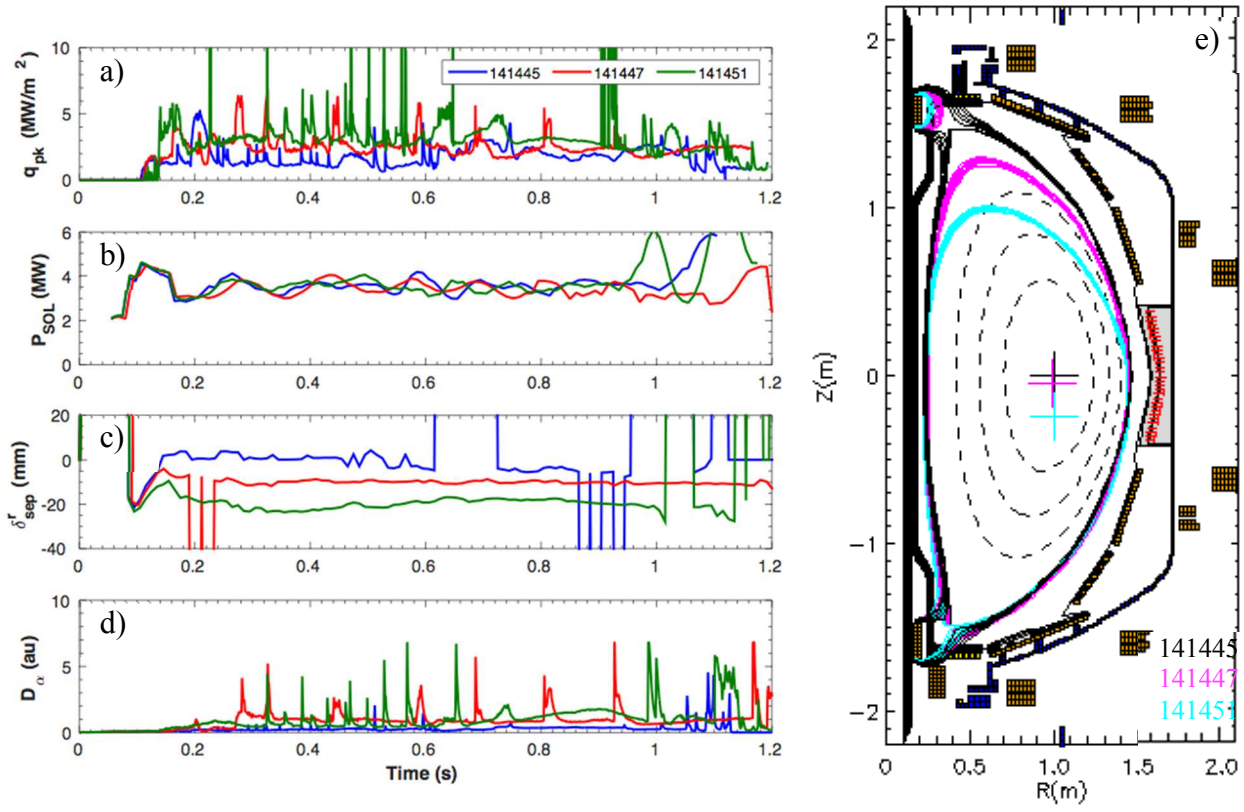

Figure 12: NSTX data showing the variation in a) peak heat flux on the lower divertor at the outer strike point; b) P_{SOL}; c) δ_r^{sep}, d) D_a in the lower divertor and e) Poloidal cross-section (t = 0.355 sec) for shots 141451 (δ_r^{sep} = -20 mm), 141447 (δ_r^{sep} = -10 mm), and 141445 (δ_r^{sep} ~ 0 mm)

equilibrium reconstruction and the lower divertor D_α respectively. Infrared coverage in NSTX was only available for the lower, outer strike point (LOSP) preventing a full accounting of the heat fluxes at each strike point. From Fig. 11a, it is clear that the inter-ELM divertor heat flux at

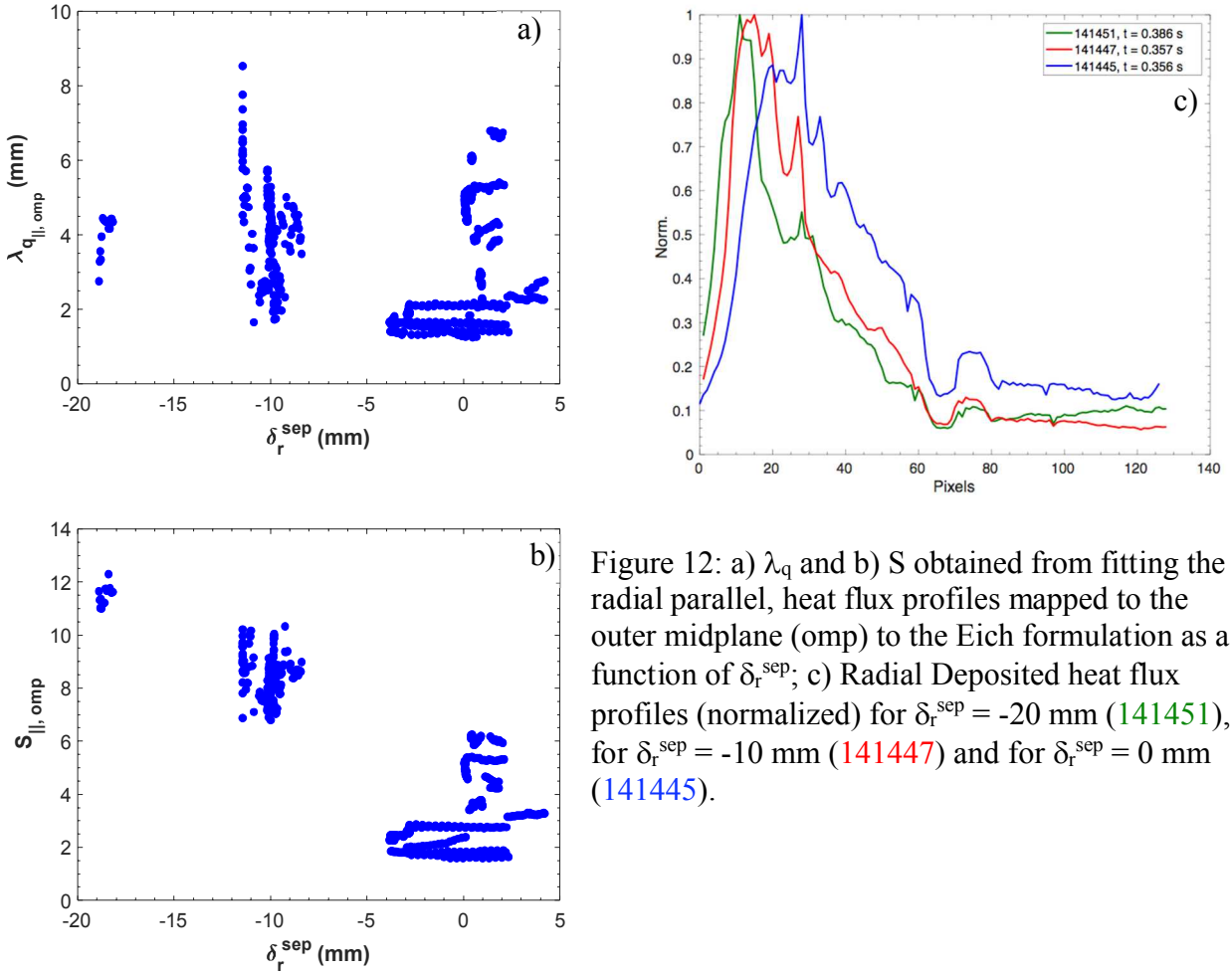

Figure 12: a) λ_q and b) S obtained from fitting the radial parallel, heat flux profiles mapped to the outer midplane (omp) to the Eich formulation as a function of δ_r^{sep}; c) Radial Deposited heat flux profiles (normalized) for δ_r^{sep} = -20 mm (141451), for δ_r^{sep} = -10 mm (141447) and for δ_r^{sep} = 0 mm (141445).

the LOSP is reduced as δ_r^{sep} approaches double-null.

The δ_r^{sep} scan also resulted in changes to the discharge shape, namely elongation κ. These variations are shown in cross-section of the poloidal magnetic field contours in Fig. 11e. The changes in κ do result in a change to the poloidal magnetic field at the outer midplane seperatrix, $B_{pol,\,omp}$ which also affects λ_q. However, the data presented here is limited to $t \leq 0.6$ sec and $B_{pol,\,omp}$ is found to vary ~ 5% between the shots analyzed over that time period and will be neglected for the remainder of this analysis.

Preliminary analysis shows that the deposited heat flux profiles, shown in Fig. 12c, broaden as δ_r^{sep} approaches 0 mm. However, it's unclear if this is due only to the change in δ_r^{sep}

or to other parameters changing such as triangularity or flux expansion in the SOL. This is resolved by calculating the parallel heat flux and mapping it to the outer midplane (OMP). Shown in Fig. 12a and b are the "Eich" Diffusive-Gaussian fits [15] of parallel heat flux data measured at the LOSP and mapped to the OMP of a) λ_q and b) S. The diffusive-gaussian fits were performed only on measurements from the LWIR band (6.5 – 10 μm). Because of the reduced divertor heat flux at DN, the signal in the individual IR bands is also reduced making the image registration process difficult and distorting the radial profile. The same procedure was used for the discharges in LSN for consistency in fitting all the IR profiles. However, the magnitude of the divertor heat fluxes are taken from the dual-band measurements.

From Fig. 12a, little change in $\lambda_{q||,\,OMP}$ is observed as a function of δ_r^{sep}. Meanwhile, $S_{||,\,OMP}$ is found to be systemically higher in LSN compared to DN discharges shown in Fig. 12b. This is qualitatively consistent with measurements made for MAST inter-ELM H-mode discharges of λ_q and S [16]. Future work on both MAST-U and NSTX-U will focus on understanding the differences in SOL transport between LSN and DN discharges and projecting to larger more powerful STs.

Total power accounting in DN discharges in NSTX is complicated since there was no IR coverage of the inner strike points and the upper divertor in general. Figure 13 shows the power deposited at the LOSP, as measured by the dual-band IR camera, normalized to P_{SOL} versus the ratio of $\delta_r^{sep}/\lambda_{q||,\,OMP}$. While P_{SOL} is shown to be constant between the discharges in Fig. 11b, this normalization is done to account for changes in P_{rad}^{core} during the shot, which has been shown to vary as

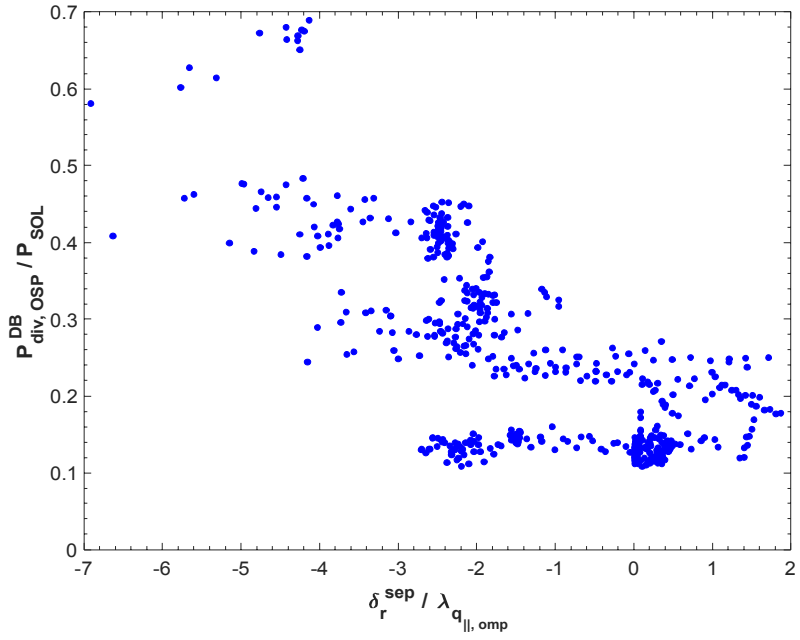

Figure 13: Ratio of deposited power at the lower, outer strike point to P_{SOL} as a function of δ_r^{sep} / $\lambda q_{||,\,omp}$.

discharge time progresses due to accumulation of carbon impurities in ELM-free NSTX discharges [17]. The ratio of $\delta_r^{sep}/\lambda_{q||,\,OMP}$ is used as a dimensionless ordering parameter. From Fig. 13, power to the LOSP is minimized for $\delta_r^{sep}/\lambda_{q||,\,OMP} \pm 2$. In this range, only 10 – 25% of P_{SOL} reaches the LOSP.

References

[1] V.A. Soukhanovskii, R. Maingi, C.E. Bush, R. Raman, R.E. Bell, R. Kaita, H.W. Kugel, C.J. Lasnier, B.P. LeBlanc, J.E. Menard, S.F. Paul, and A.L. Roquemore. "Divertor heat flux reduction and detachment experiments in NSTX",J. Nucl. Mater., 363-365:432, 2007.

[2] V. A. Soukhanovskii, R. Maingi, D. A. Gates, J. E. Menard, S. F. Paul, R. Raman, A. L. Roquemore, M. G. Bell, R. E. Bell, J. A. Boedo, C. E. Bush, R. Kaita, H. W. Kugel, B. P. LeBlanc, D. Mueller, and the NSTX Team. "Divertor heat flux mitigation in the National Spherical Torus Experiment", *Phys. Plasmas*, 16, (2009).

[3] V. A. Soukhanovskii, R. Maingi, D. A. Gates , J. E. Menard, S. F. Paul, R. Raman, A. L. Roquemore, R. E. Bell, C. E. Bush, R. Kaita, H. W. Kugel, B. P. LeBlanc, D. Mueller, "Divertor Heat Flux Mitigation in High-Performance H-mode Plasmas in the National Spherical Torus Experiment", Nuclear Fusion, 49, 095025 (2009).

[4] V.A. Soukhanovskii, D.W. Johnson, R. Kaita, and A.L. Roquemore. "Electron density measurements in the National Spherical Torus Experiment detached divertor region using Stark broadening of deuterium infrared Paschen emission lines", Rev. Sci. Instrum., 77:10127, 2006.

[5] F. Scotti, V.A. Soukhanovskii, M.L. Adams, H.A. Scott, H. W. Kugel, R. Kaita and A.L. Roquemore, "Observation and modeling of inner divertor re-attachment in discharges with lithium coatings in NSTX", Journal of Nuclear Materials, Volume 415, Issue 1, Supplement, 1 August 2011, Pages S405-S408

[6] Maingi, R; Bush, CE; Kaita, R, *et al*. "Divertor heat flux scaling with heating power and plasma current in H-mode discharges in the National Spherical Torus eXperiment", *J. Nucl. Mater.*, **363**, 196-200, (2007).

[7] T. K. Gray, R. Maingi, V. A. Soukhanovskii, J. E. Surany, J.-W. Ahn, and A. G. McLean, "Dependence of divertor heat flux widths on heating power, flux expansion, and plasma current in the NSTX", J. Nucl. Mater., vol. 415, no. 1, pp. S360–S364, 2011.

[8] V.A.Soukhanovskii, R.Maingi, R.E.Bell, C.E.Bush, D.A.Gates, R.Kaita, H.W.Kugel, B.P.LeBlanc, R.Maqueda, J.E.Menard, D.Mueller, S.F.Paul, R.Raman, A.L.Roquemore, "High flux expansion divertor studies in NSTX", in 36th EPS Conf. on Plasma Phys., Sofia, Bulgaria, 2009, Paper P2.178, http://arxiv.org/abs/0912.4281.

[9] M. A. Makowski, D. Elder, T. K. Gray, B. LaBombard, C. J. Lasnier, A. W. Leonard, R. Maingi, T. H. Osborne, P. C. Stangeby, J. L. Terry, and J. Watkins, "Analysis of a multi-machine database on divertor heat fluxes", Phys. Plasmas **19**, 056122 (2012)

[10] Final Report on the DOE OFES FY 2010 Joint Research Target on thermal SOL transport research, by Alcator C-Mod, DIII-D and NSTX staff

[11] T. K. Gray, et al. J. Nucl. Mater. **415** (2011) S360-S364

[12] R. Maingi, et al. J. Nucl. Mater. **337-339** (2005) 727-731

[13] J.-W. Ahn, et al. Rev. Sci. Instrum. **81** (2010) 023501

[14] A.G. McLean, et al. Rev. Sci. Instrum. **83** (2012) 053706

[15] T. Eich, et al. Phys. Rev. Lett. **107** (2011) 215001

[16] J.R. Harrison, et al. J. Nucl. Mater. **438** (2013) S375-S378

[17] M. Podesta, et al. Nucl. Fusion. **52** (2012) 033008